



Contents lists available at ScienceDirect

# Spectrochimica Acta Part A: Molecular and Biomolecular Spectroscopy

journal homepage: [www.elsevier.com/locate/saa](http://www.elsevier.com/locate/saa)

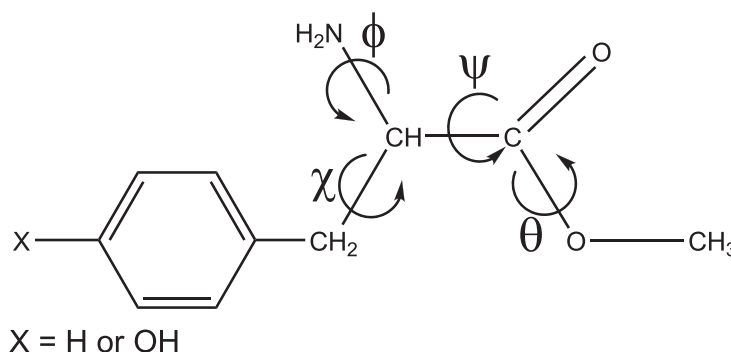
## Phenylalanine and tyrosine methyl ester intramolecular interactions and conformational analysis by $^1\text{H}$ NMR and infrared spectroscopies and theoretical calculations

Rodrigo A. Cormanich<sup>a</sup>, Lucas C. Ducati<sup>b</sup>, Cláudio F. Tormena<sup>a</sup>, Roberto Rittner<sup>a,\*</sup><sup>a</sup>Chemistry Institute, University of Campinas, P.O. Box 6154, 13083-970 Campinas, Brazil<sup>b</sup>Chemistry Institute, University of São Paulo, P.O. Box 26077, 05508-900 São Paulo, Brazil

### HIGHLIGHTS

- Phenylalanine and tyrosine were investigated by theoretical and experimental methods.
- The lowest energy conformers are not stabilized by hydrogen bonding.
- Steric and hyperconjugative effects were analyzed for all conformers.
- Several theoretical methods were used to explain the conformational preferences.

### GRAPHICAL ABSTRACT



### ARTICLE INFO

#### Article history:

Received 25 September 2013

Received in revised form 29 November 2013

Accepted 21 December 2013

Available online 3 January 2014

#### Keywords:

Conformational analysis  
 Amino acid methyl ester derivatives  
 $^1\text{H}$  NMR spectroscopy  
 Infrared spectroscopy  
 Intramolecular hydrogen bonding  
 Stereoelectronic effects

### ABSTRACT

Amino acid conformational analysis in solution are scarce, since these compounds present a bipolar zwitterionic structure ( $^+\text{H}_3\text{N}-\text{CHR}-\text{COO}^-$ ) in these media. Also, intramolecular hydrogen bonds have been classified as the sole interactions governing amino acid conformational behavior in the literature. In the present work we propose phenylalanine and tyrosine methyl ester conformational studies in different solvents by  $^1\text{H}$  NMR and infrared spectroscopies and theoretical calculations. Both experimental and theoretical results are in agreement and suggest that the conformational behavior of the phenylalanine and tyrosine methyl esters are similar and are dictated by the interplay between steric and hyperconjugative interactions.

© 2014 Elsevier B.V. All rights reserved.

### Introduction

The understanding of amino acids conformational behavior in solution is essential for a deep recognition of the complex protein geometries to which such compounds give rise [1–4]. However, intramolecular hydrogen bonds (IHB) have been commonly

considered the sole interaction governing amino acid conformational isomerism since the very beginning of amino acid conformational studies in the literatures [5–18]. Recently, it was found that the balance between steric and hyperconjugative effects and not IHBs are actually the main forces dictating the conformational behavior of a considerable range of amino acids and amino acid esters [19–23].

Moreover, few to none conformational studies of amino acids in solution can be found in the literature, particularly using NMR

\* Corresponding author. Tel./fax: +55 19 3521 3150; fax: +55 19 3521 3023.  
 E-mail address: [rittner@iqm.unicamp.br](mailto:rittner@iqm.unicamp.br) (R. Rittner).

spectroscopy. The main reason is that amino acids in solution present a bipolar zwitterion structure ( $^+H_3N-CHR-COO^-$ ), which is a rough approximation for the understanding of the behavior of an amino acid residue in a polypeptide or protein environment [24–26]. Consequently, experimental amino acid conformational studies have been almost limited to gas phase based spectroscopies. Although many improvements were recently achieved by gas phase methods, these cannot yet determine the nature and quantitative distributions of amino acid conformers. Also, since amino acid compounds are thermally unstable and have high melting points and low vapor pressures, the vaporization of amino acid compounds with large side chains is a challenge for such techniques [27–29].

Therefore, in the present work, phenylalanine and tyrosine methyl ester derivatives conformational behavior in solution was studied, which does not exhibit the bipolar zwitterionic structure and also show considerable solubility in the majority of organic solvents, by  $^1H$  NMR spectroscopy. The obtained experimental  $^3J_{HH}$  spin–spin coupling constants (SSCCs) were compared with theoretical calculations in the framework of the quantum theory of atoms in molecules (QTAIM) [30] and the natural bond orbitals (NBO) analysis [31].

## Materials and methods

### Computational details

The phenylalanine methyl ester (phe-OMe) and tyrosine methyl ester (tyr-OMe) conformers were obtained by scanning the  $\chi$  [ $C(Ph)-CH_2-CH-C(O)$ ] dihedral angle in  $10^\circ$  steps from  $0^\circ$  to  $360^\circ$  and using the 6 conformers previously obtained for ala-OMe compound,  $\phi$  [ $n_N-N-C-C(O)$ ] and  $\psi$  ( $N-C-C=O$ ) dihedral angles [22] (dihedral angle representation showed in Fig. 1). Each potential energy curve (PEC) showed 3 minima (Figs. S1 and S2; Supporting information), which were subsequently optimized at the B3LYP/aug-cc-pVDZ theoretical level. Frequency calculations showed that all conformers, except **IIIa** and **IV2c**, had no imaginary frequencies for both phe-OMe and tyr-OMe and are true energy minima in each PEC. Thus, the resulting 16 conformers of the phe-OMe and tyr-OMe compounds were optimized by using the integral equation formalism polarizable continuum model (IEF-PCM) [32] in three different dielectric constants ( $\epsilon$ ): chloroform ( $\epsilon = 4.8$ ), acetonitrile ( $\epsilon = 37.5$ ) and DMSO ( $\epsilon = 46.7$ ). From these IEF-PCM calculations the  $^3J_{HH}$  spin–spin coupling constants were obtained for each conformer using the B3LYP functional and the EPR-III basis set [33]. The intramolecular interactions were evaluated using the natural bond orbitals (NBO) and the quantum theory of atoms in molecules (QTAIM) methods with the obtained B3LYP/aug-cc-pVDZ electronic density optimization calculations. The QTAIM integrated Laplacian  $\rho$  values over each atomic basin ( $\Omega$ ) were always less than  $10^{-3}$  atomic units (au) for all atoms and indicate good integrated atomic properties. PEC, optimization, IEF-PCM and NBO calculations were carried out in the Gaussian03

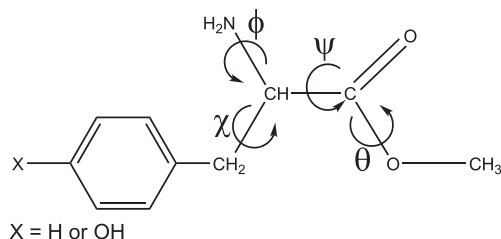


**Fig. 1.** The  $\phi$  [ $n_N-N-C-C(O)$ ],  $\psi$  ( $N-C-C=O$ ),  $\theta$  ( $CH_3-O-C=O$ ) and  $\chi$  ( $Ha-C-C-Hb$ ) dihedral angle representations.

package of programs [34] and the QTAIM calculations were obtained from the AIMALL software [35].

### Amino acid methyl ester chloridrate deprotonation

The L-phe-OMe and the L-tyr-OMe were commercially available (Acros Organics) as a chloridrate (phe-OMe-HCl and L-tyr-OMe-HCl) and were deprotonated using commercial zinc dust [36]. To produce a suspension, commercial zinc dust (100 mg) was added to the phe-OMe-HCl and L-tyr-OMe-HCl (1 mmol) in 10 mL of  $CH_2Cl_2$  and THF, respectively. The mixture was stirred for ca. 10 min. Subsequently, the mixture was filtered and the solvent was evaporated. The resultant phe-OMe and tyr-OMe were obtained as a free ester crystalline solid.

### $^1H$ NMR spectra

The phe-OMe and tyr-OMe  $^1H$  NMR experiments were recorded on a Bruker Avance-III spectrometer operating at 400.13 MHz. Spectra were recorded in solutions of ca. 10 mg in 0.7 mL of deuterated commercial solvents without further purification:  $CDCl_3$ ,  $CD_2Cl_2$ , THF, pyridine- $d_5$ , acetone- $d_6$ , methanol- $d_4$ , acetonitrile- $d_3$  and DMSO- $d_6$ , referenced to internal TMS. The typical conditions used were as follows: a probe temperature of  $25^\circ C$ , 16 transients, a spectral width of 2.6 kHz, 64k data points, an acquisition time of 12.6 s and zero-filled to 128k points ( $^1H$  NMR spectra are provided in the Supporting information section).

### Infrared spectra

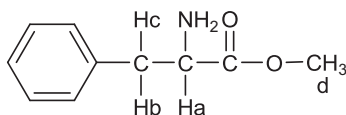
Phe-OMe and tyr-OMe samples were prepared with a concentration of 0.03 M in  $CHCl_3$ ,  $CH_3CN$  and DMSO dried solvents. The infrared spectra were recorded on a FTIR Shimadzu IRPrestige-21 spectrometer by using a 0.5 mm width NaCl round cell window. The infrared spectrometer conditions used were the following: number of scans = 64, resolution =  $1\text{ cm}^{-1}$ , spectra range =  $400\text{--}4000\text{ cm}^{-1}$ . The equipment was purged with dry nitrogen gas. Deconvolution of the  $C=O$  absorption bands were carried out by using the GRAMS curve fitting software [37].

## Results and discussions

The  $^1H$  NMR spectra for the deprotonated phe-OMe and tyr-OMe were obtained in different solvents (spectra are shown in the Supporting information): apolar ( $CDCl_3$ ,  $CD_2Cl_2$ , THF- $d_8$ ), polar aprotic (pyridine- $d_5$ , acetone- $d_6$ , acetonitrile- $d_3$  and DMSO- $d_6$ ) and polar protic (methanol- $d_4$ ) solvents. The  $^3J_{HH}$  values were recorded and their values for the phe-OMe compound are shown in Table 1. Fig. 2 shows the three conformational minima (**a**, **b** and **c**) expected for the side chain in relation to the main chain for the phe-OMe. The **a** and **b** geometries have an *anti* relationship between the hydrogens Ha and Hb and Ha and Hc, respectively, while the **c** geometry has a *gauche* relationship between Ha and Hb and between Ha and Hc (Fig. 2). In this way, based in the Karplus relationship [38], one would expect that the  $^3J_{HaHb}$  and the  $^3J_{HaHc}$  spin–spin coupling constants to have higher values for conformers with the **a** and **b** geometries, respectively, and smaller values for conformers with the **c** geometry. Table 1 shows that the  $^3J_{HaHb}$  values decrease with the increase of the dielectric constant ( $\epsilon$ ) of the solvent, while the  $^3J_{HaHc}$  values show the opposite behavior, i.e., the  $^3J_{HaHc}$  values increase with the increase of the dielectric constant value. This pattern is interesting and shows that in non-polar solvents  $^3J_{HaHb}$  and  $^3J_{HaHc}$  values are far one from each other, while in solvents with higher values of dielectric constant, the two coupling constant values are the same. Thus, two different hypotheses could explain the

**Table 1**

Experimental  $^1\text{H}$  NMR chemical shift values (ppm) and SSCCs (Hz) for the phe-OMe compound in different solvents.



Solvent	$\epsilon$	$\delta\text{Ha}$	$\delta\text{Hb}$	$\delta\text{Hc}$	$\delta\text{Hd}$	$^3J_{\text{HaHb}}$	$^3J_{\text{HaHc}}$	$^2J_{\text{HbHc}}$
$\text{CDCl}_3$	4.8	4.10	3.09	3.25	3.72	7.9	4.8	14.0
$\text{CD}_2\text{Cl}_2$	9.8	4.13	3.13	3.27	3.78	7.6	4.9	14.1
Pyridine- $\text{d}_5$	12.3	3.90	2.99	3.15	3.61	7.4	5.7	13.4
Acetone- $\text{d}_6$	20.7	4.15	3.21	3.28	3.70	6.5	5.2	13.8
Methanol- $\text{d}_4^a$	32.7	3.95	3.11	3.11	3.37	6.6	6.6	–
$\text{CD}_3\text{CN}$	37.5	4.00	3.08	3.15	3.67	6.1	6.1	13.9
$\text{DMSO-}d_6^a$	46.7	3.66	2.88	2.88	3.57	6.7	6.7	–

<sup>a</sup> In methanol- $\text{d}_4$  and  $\text{DMSO-}d_6$  Hb and Hc cannot be distinguished.

$^3J_{\text{HaHb}}$  and the  $^3J_{\text{HaHc}}$  values in different solvents: one is that the conformational equilibrium would be displaced progressively to c geometry conformers with the increase of the dielectric constant, so this could be the explanation for the  $^3J_{\text{HaHb}}$  and the  $^3J_{\text{HaHc}}$  values approaching each other when the dielectric constant value increases. The other hypothesis is: with the progressive increase of the dielectric constant, conformers with b geometries are being favored over a geometry conformers until the  $^3J_{\text{HaHb}}$  and the  $^3J_{\text{HaHc}}$  values become equal.

In order to get a deeper insight into the obtained experimental results, theoretical calculations were carried out. Both the phe-OMe and tyr-OMe conformer names were classified with Arabic numerals followed by the letters a, b or c. The numerals indicate the main chain geometry taken from the ala-OMe [22] and the letters indicate the side chain geometries as shown in Fig. 2. From the constructed PECs (Supporting information), 18 conformers for both phe-OMe and tyr-OMe were obtained. At the B3LYP/aug-cc-pVDZ theoretical level the IIIa and IV2c phe-OMe and tyr-OMe conformers are not true minima and were discarded from the set of 18 conformers. Thus, both phe-OMe and tyr-OMe have 16 conformers each, which are shown in Figs. S3 and S4 (Supporting information) and the phe-OMe energies are shown in Table 2. Each of the 16 conformers was reoptimized by using the implicit solvent IEF-PCM model with chloroform, acetonitrile and DMSO dielectric constant values (Table 2 shows the values obtained for phe-OMe). The  $^3J_{\text{HaHb}}$  and the  $^3J_{\text{HaHc}}$  SSCCs theoretical values were obtained for each conformer in the IEF-PCM implicit solvent model by using the B3LYP/EPR-III level.

The contribution of each “i” conformer in a given solvent for the observed  $^3J_{\text{HaHb}}$  SSCC may be estimated through the following equation:

$$^3J_{\text{HH}} = \sum_{i=1}^n \frac{\eta_i}{\eta_T} ^3J_i \quad (1)$$

with  $\eta_i/\eta_T$  representing the relative population of the conformer “i” and  $^3J_i$  the intrinsic  $^3J_{\text{HaHb}}$  or  $^3J_{\text{HaHc}}$  value of the conformer “i”. The obtained  $\eta_i/\eta_T$  value multiplied by the  $^3J_{\text{HaHb}}$  or  $^3J_{\text{HaHc}}$  for each phe-OMe conformer in each solvent is depicted in Fig. 3a and b, respectively, which show considerable value variations going from one solvent to another. Fig. 3c and d shows the calculated  $^3J_{\text{HaHb}}$  and  $^3J_{\text{HaHc}}$  values for each conformer and indicate that the variations of these SSCCs in different solvents are negligible. Thus, the variations observed in Fig. 3a and b are indicative of the phe-OMe conformer relative population ( $\eta_i/\eta_T$  parameter) changes in each solvent. From the simultaneous observation of Fig. 3a and b, one may conclude that the second hypothesis is the correct one, i.e., the most stable conformers Ia and Ib acquire similar  $\eta_i/\eta_T$  values with the increase of the solvent dielectric constant. Some small populational variations may be observed in Fig. 3a and b for the other conformers, but these may be considered as secondary effect.

It was also recorded experimental infrared spectra for the phe-OMe and tyr-OMe compounds. Table 3 shows the obtained phe-OMe C=O absorption bands in  $\text{CHCl}_3$ ,  $\text{CH}_3\text{CN}$  and  $\text{DMSO}$  solvents. Those bands could, in principle, be deconvoluted in all phe-OMe 16 conformers which give origin of each C=O absorption band. However, in practice, each experimental C=O band has only 3 components which could be used in the deconvolution procedure. Hence, one can deduce that each of those components could be attributed to set of conformers. In this way, there were obtained theoretical harmonic C=O stretching values for each phe-OMe conformer (Table 2), which, in order to account for anharmonic vibrational effects, were corrected by using different values of correction factors (CF), and those were distributed in three different sets A, B and C. The criterion of distribution of conformers in each set was the C=O stretching values (Table 2), i.e., conformers with close C=O absorption values were grouped in the sets A (intermediate values), B (smaller values) and C (higher values). Remarkably, the sum of the theoretically obtained conformer population values in each set is in excellent agreement with experiment (Table 3). Also, the theoretical C=O absorption values obtained for each set, which is given by the following equation:

$$\text{Group}_{\text{C=O}} = \sum_{i=1}^n \%P \times \text{conformer}(i)_{\text{C=O}} \quad (2)$$

with  $\text{Group}_{\text{C=O}}$  and  $\text{conformer}(i)_{\text{C=O}}$  representing the values of the C=O stretching frequency for each group (A, B and C) and of the “i” conformers pertaining to each group, respectively, are in agreement with the experimental ones (Table 3). Then, both experimental  $^1\text{H}$  NMR and infrared theoretical data are in agreement with the theoretical results. The theoretical data, in turn, explains the experimental results.

The next step is the analysis of the intramolecular effects which give rise to the phe-OMe conformational preferences. In this way, the QTAIM and the NBO methods were applied. The phe-OMe QTAIM molecular graphs are displayed in the Supporting

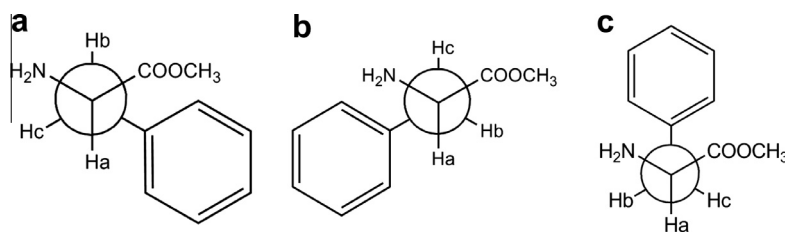


Fig. 2. Newman projections for the a, b and c phe-OMe possible side chain geometries.

**Table 2**

Relative energies<sup>a</sup> (kcal mol<sup>-1</sup>), populations (percentage) for the phe-OME conformers in the gas phase (B3LYP/aug-cc-pVDZ) and by using the IEF-PCM implicit model in CHCl<sub>3</sub>, CH<sub>3</sub>CN and DMSO. Theoretical (B3LYP/aug-cc-pVDZ) C=O stretching values are also showed.

Conformer	Isolated		CHCl <sub>3</sub>			CH <sub>3</sub> CN			DMSO		
	ΔE	%P	ΔE	%P	C=O <sup>1</sup>	ΔE	%P	C=O <sup>2</sup>	ΔE	%P	C=O <sup>3</sup>
Ia	0.00	20.6	0.00 <sup>A</sup>	25.5	1733.4	0.00 <sup>A</sup>	15.1	1741.8	0.01 <sup>A</sup>	21.1	1732.7
Ib	0.16	15.8	0.18 <sup>A</sup>	18.6	1736.8	0.00 <sup>A</sup>	15.1	1745.9	0.00 <sup>A</sup>	21.4	1736.6
Ic	0.26	13.3	0.66 <sup>A</sup>	8.4	1741.5	0.74 <sup>A</sup>	6.9	1748.3	0.86 <sup>A</sup>	5.0	1739.7
IIIb	1.41	1.9	1.08 <sup>B</sup>	4.1	1727.6	0.76 <sup>B</sup>	6.8	1731.9	0.76 <sup>B</sup>	5.9	1723.4
IIIc	0.95	4.2	1.38 <sup>B</sup>	2.5	1723.7	1.51 <sup>B</sup>	3.1	1730.7	1.61 <sup>B</sup>	1.4	1719.9
IV1a	0.93	4.3	0.72 <sup>C</sup>	7.6	1742.1	0.56 <sup>C</sup>	8.4	1749.7	0.54 <sup>C</sup>	8.6	1741.8
IV1b	0.08	18.0	0.30 <sup>C</sup>	15.4	1745.9	0.19 <sup>C</sup>	12.3	1753.6	0.24 <sup>C</sup>	14.3	1744.9
IV1c	1.86	0.9	1.73 <sup>C</sup>	1.4	1750.3	1.30 <sup>C</sup>	3.8	1755.5	1.23 <sup>C</sup>	2.7	1746.2
IV2a	2.74	0.2	2.84 <sup>C</sup>	0.2	1733.1	1.50 <sup>C</sup>	3.1	1753.3	1.52 <sup>C</sup>	1.7	1742.5
IV2b	0.36	11.2	0.80 <sup>C</sup>	6.6	1741.9	0.77 <sup>C</sup>	6.7	1750.9	0.74 <sup>C</sup>	6.1	1742.4
V1a	2.26	0.5	2.29 <sup>C</sup>	0.5	1752.2	1.79 <sup>C</sup>	2.3	1756.1	1.52 <sup>C</sup>	1.6	1743.6
V1b	0.83	5.1	1.42 <sup>A</sup>	2.3	1740.7	1.51 <sup>A</sup>	3.1	1746.8	1.55 <sup>A</sup>	1.6	1738.8
V1c	2.97	0.1	3.27 <sup>B</sup>	0.1	1728.5	3.06 <sup>B</sup>	0.6	1731.8	3.11 <sup>B</sup>	0.1	1723.8
V2a	2.55	0.3	1.76 <sup>C</sup>	1.3	1749.1	1.11 <sup>C</sup>	4.7	1749.6	1.12 <sup>C</sup>	3.2	1741.6
V2b	1.10	3.2	0.97 <sup>A</sup>	4.9	1736.4	0.82 <sup>A</sup>	6.4	1741.7	0.91 <sup>A</sup>	4.6	1732.6
V2c	2.28	0.4	2.17 <sup>B</sup>	0.7	1729.6	2.10 <sup>B</sup>	1.7	1737.7	2.08 <sup>B</sup>	0.6	1727.3

<sup>a</sup> Zero point energy correction included.

<sup>1</sup> It was applied a CF of 0.989.

<sup>2</sup> It was applied a CF of 0.998.

<sup>3</sup> It was applied a CF of 0.993.

<sup>A</sup> group A conformers.

<sup>B</sup> group B conformers.

<sup>C</sup> group C conformers.

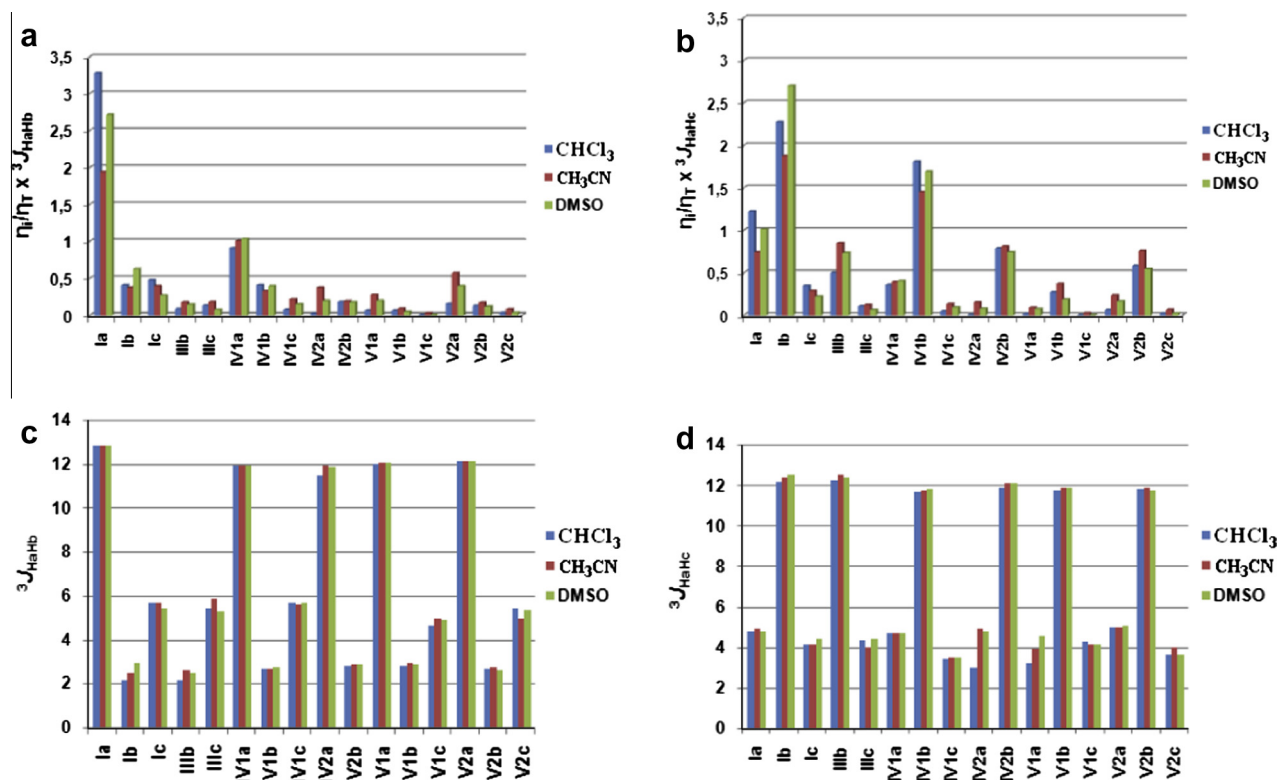


**Fig. 3.** Calculated (B3LYP/aug-cc-pVDZ level in the IEF-PCM implicit solvent model) phe-OME conformer parameter variations in different solvents for (a)  $\eta_i/\eta_T \times {}^3J_{\text{HaHb}}$ , (b)  $\eta_i/\eta_T \times {}^3J_{\text{HaHc}}$ , (c)  ${}^3J_{\text{HaHb}}$  and (d)  ${}^3J_{\text{HaHc}}$ .

Information and indicate that an IHB is formed in the main chain for all conformers, but that non-usual C—H...O interactions are also formed between the side chain and the main chain geometries for conformers **Ic**, **V2a** and **V2c**. However, conformer **Ic** forms a very weak C—H...O interaction, which does not fulfill the Popelier criteria [39] (Table 4). Thus, non-negligible C—H...O interactions are formed only by conformers **V2a** and **V2c**, which are of high

relative energy and correspond to small populations (Table 2). Therefore, an IHB is present only in low populated conformers and, hence, have a secondary role in the conformational behavior of phe-OME according to QTAIM calculations. On the other hand, the  $\Delta E_{\text{Lewis}}$  (conformer energy without hyperconjugation) and  $\Delta E_{\text{hyper}}$  (total hyperconjugation energy) values (Table 5), obtained by the NBO method, indicate that the interplay between steric

**Table 3**  
Deconvolution of the experimental C=O bond stretching absorption bands obtained by experimental infrared spectra in CHCl<sub>3</sub>, CH<sub>3</sub>CN and DMSO solvents of the phe-OMe compound. Experimental and theoretical values of the C=O bond stretching (cm<sup>-1</sup>) and population (%) for each A, B and C group are also reported.

CHCl <sub>3</sub>				CH <sub>3</sub> CN				DMSO				
Theoretical		Experimental		Theoretical		Experimental		Theoretical		Experimental		
C=O <sup>1</sup>	%P	C=O	%P	C=O <sup>2</sup>	%P	C=O	%P	C=O <sup>3</sup>	%P	C=O	%P	
<b>Group A</b>	1736.1	59.8	1737.0	55.0	1744.4	46.5	1743.0	46.7	1735.1	53.7	1735.3	56.5
<b>Group B</b>	1726.7	7.4	1725.8	7.8	1736.6	15.2	1737.0	18.0	1723.1	8.1	1725.4	9.6
<b>Group C</b>	1745.9	32.8	1745.9	37.2	1752.1	38.3	1752.0	35.3	1743.5	38.2	1743.4	33.9

<sup>1</sup> It was applied a correction factor (CF) of 0.989.

<sup>2</sup> It was applied a correction factor (CF) of 0.998.

<sup>3</sup> It was applied a correction factor (CF) of 0.993.

**Table 4**  
Popelier parameters applied to the phe-OMe conformers which form CH...O interactions. The  $\rho_{\text{HBOP}}$ ,  $\nabla^2\rho_{\text{HBOP}}$  and all integration parameters obtained for hydrogen atoms are in atomic units (au). The conformer **1a** is used as reference, since it cannot form a CH...O interaction.

Conformer	$\rho_{\text{HBOP}}$	$\nabla^2\rho_{\text{HBOP}}$	$q(\text{H})$	$E(\text{H})$	$M_1(\text{H})$	$V(\text{H})$
<b>1a</b>	–	–	<b>+0.004</b>	<b>-0.6126</b>	<b>0.131</b>	<b>49.64</b>
<b>1c</b>	0.004	+0.016	-0.006	-0.6175	0.124	50.19
<b>V2a</b>	0.007	+0.026	+0.025	-0.6060	0.123	46.69
<b>V2c</b>	0.006	+0.021	+0.011	-0.6110	0.125	48.13

**Table 5**  
Full energy of the real system ( $\Delta E_{\text{FULL}}$ )<sup>a</sup>, energy of the hypothetical case where hyperconjugation is removed ( $\Delta E_{\text{Lewis}}$ ) and hyperconjugative energy ( $\Delta E_{\text{hyper}}$ ) for the phe-OMe conformers. Energy values in kcal mol<sup>-1</sup>.

	<b>1a</b>	<b>1b</b>	<b>1c</b>	<b>IIIb</b>	<b>IIIc</b>	<b>IV1a</b>	<b>IV1b</b>	<b>IV1c</b>
$\Delta E_{\text{Full}}$	0.00	0.16	0.26	1.41	0.95	0.93	0.08	1.86
$\Delta E_{\text{Lewis}}$	5.87	3.34	8.38	4.09	10.83	7.10	4.97	10.67
$\Delta E_{\text{hyper}}$	8.03	5.27	10.36	4.71	12.20	8.27	7.06	10.86
	<b>IV2a</b>	<b>IV2b</b>	<b>V1a</b>	<b>V1b</b>	<b>V1c</b>	<b>V2a</b>	<b>V2b</b>	<b>V2c</b>
$\Delta E_{\text{Full}}$	2.74	0.36	2.26	0.83	2.97	2.55	1.10	2.28
$\Delta E_{\text{Lewis}}$	4.77	1.50	0.14	0.00	6.40	4.47	3.92	12.83
$\Delta E_{\text{hyper}}$	4.02	3.20	0.00	1.24	5.44	4.19	5.01	12.74

<sup>a</sup> ZPE corrections included.

effects and hyperconjugative effects are important in determining the phe-OMe conformational preferences.

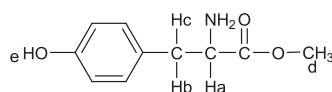
It is expected that deviations from 0° and/or 180° for a conformer  $\psi$  and  $\phi$  dihedral angles occur in order to decrease steric effects between two atoms or group of atoms, followed by the consequent decrease of hyperconjugative effects, since the more linear the bonds in one conformer the better the orbital superpositions [19]. Table 6 presents the phe-OMe  $\psi$ ,  $\phi$  and  $\chi$  dihedral angle values. In all cases, conformers with **c** side chain geometry have a lower deviation from 0°/180° for the dihedral angle  $\psi$  in comparison with conformers with **a** and **b** side chain geometries, and conformers with **b** geometry are the ones which show the greatest deviations. These results are in agreement with the  $\Delta E_{\text{Lewis}}$  and  $\Delta E_{\text{hyper}}$  values shown in Table 5, i.e., conformers with **c** geometry have higher stabilization by hyperconjugative effects, since they have the smallest  $\psi$  and  $\phi$  deviation values from 0°/180°, while

**Table 6**  
 $\psi$ ,  $\phi$  and  $\chi$  dihedral angle values for the phe-OMe conformers calculated at the B3LYP/aug-cc-pVDZ theoretical level.

Conformer	$\psi$ [N–C–C=O]	$\phi$ [ $n_{\text{N}}\text{–N–C–C(O)}$ ]	$\chi$ [Hb–CH–C–Ha]
<b>1a</b>	59.2	173.8	62.6
<b>1b</b>	24.6	163.5	165.4
<b>1c</b>	4.4	181.3	295.0
<b>IIIb</b>	219.7	170.6	163.3
<b>IIIc</b>	184.4	182.7	292.1
<b>IV1a</b>	54.9	64.6	63.9
<b>IV1b</b>	35.0	72.7	177.4
<b>IV1c</b>	22.4	74.3	297.4
<b>IV2a</b>	335.7	84.7	80.5
<b>IV2b</b>	343.5	83.2	175.5
<b>V1a</b>	241.5	51.0	58.4
<b>V1b</b>	221.9	59.7	172.4
<b>V1c</b>	198.2	59.7	296.2
<b>V2a</b>	108.7	58.6	75.3
<b>V2b</b>	138.1	63.8	173.0
<b>V2c</b>	172.7	79.9	299.7

conformers with **b** geometry have the greatest deviations and, hence, lower values of  $\Delta E_{\text{Lewis}}$  (and consequently are less stabilized by hyperconjugative effects). Conformers with **b** geometry are in general the most stable, while conformers with **c** geometry are the least stable. Thus, one may conclude that steric effects are more important than hyperconjugative effects for the phe-OMe conformational preferences. Notwithstanding, although steric effects have a more important role, the balance between steric and hyperconjugative effects determine the phe-OMe conformational energies from the NBO viewpoint.

The only difference between phe-OMe and tyr-OMe is a hydroxyl group attached to the aromatic ring at the *para* position in relation to the aminoester main chain geometry. Thus, due to the distance between the hydroxyl group and the main chain geometry, a similar conformational behavior for tyr-OMe in comparison with phe-OMe is expected. However, the hydroxyl group reduces considerably the tyr-OMe solubility in organic solvents of low dielectric constant in comparison with the phe-OMe compound and, hence, it is possible that these compounds might have a different behavior in solution. Indeed, tyr-OMe is not soluble in both chloroform and dichloromethane and these two solvents were replaced by THF, which is the most non-polar solvent in which the

**Table 7**Experimental  $^1\text{H}$  NMR chemical shift values (ppm) and SSCCs (Hz) for the tyr-OMe compound in different solvents.

Solvent	$\epsilon$	$\delta\text{Ha}$	$\delta\text{Hb}$	$\delta\text{Hc}$	$\delta\text{Hd}$	$\delta\text{He}$	$^3J_{\text{HaHb}}$	$^3J_{\text{HaHc}}$	$^2J_{\text{HbHc}}$
THF- $\text{d}_8$	7.6	4.10	3.04	3.12	3.65	–	6.5	5.3	13.8
Pyridine- $\text{d}_5$	12.3	3.86	2.97	3.10	3.60	11.37	7.1	5.8	13.5
Acetone- $\text{d}_6$	20.7	4.12	3.16	3.23	3.73	–	6.2	5.7	14.0
Methanol- $\text{d}_4^a$	32.7	3.88	3.00	3.04	4.87	–	6.4	6.4	13.9
$\text{CD}_3\text{CN}$	37.5	3.98	3.04	3.09	3.71	–	5.9	6.1	14.2
$\text{DMSO-}d_6^a$	46.7	3.61	2.77	2.77	3.57	9.24	6.6	6.6	–

<sup>a</sup> In methanol- $\text{d}_4$  and  $\text{DMSO-}d_6$  Hb and Hc are undistinguishable.

tyr-OMe can be solubilized. Thus, the tyr-OMe  $^1\text{H}$  NMR parameters were recorded in the solvents shown in Table 7, which shows a considerable SSCC value variation with the solvent as well as for phe-OMe. Moreover, the  $^3J_{\text{HaHb}}$  and  $^3J_{\text{HaHc}}$  values show the same trend observed for phe-OMe, i.e., these two SSCCs have different values in solvents of low dielectric constant and become more similar to each other, in more polar solvents, until they reach the same values in DMSO.

Analogously to the phe-OMe compound, tyr-OMe has 16 true energy minima, which were optimized at the B3LYP/aug-cc-pVDZ theoretical level, in the isolated state, and by using the IEF-PCM implicit solvent model for chloroform, acetonitrile and DMSO dielectric constant values (Table 8). The  $\eta_i/\eta_T$  multiplied by  $^3J_{\text{HaHb}}$  and  $^3J_{\text{HaHc}}$  values calculated at the B3LYP/EPR-III level for chloroform, acetonitrile and DMSO dielectric constants are depicted in Fig. 4a and b, showing considerable variations for the calculated solvents, together with  $^3J_{\text{HaHb}}$  and  $^3J_{\text{HaHc}}$  single values (Fig. 4c and d, respectively), which are constant with the solvent variation. The  $\eta_i/\eta_T$  multiplied by  $^3J_{\text{HaHb}}$  for the conformer **Ia** and the  $\eta_i/\eta_T$  multiplied by  $^3J_{\text{HaHc}}$  for the conformer **Ib** (Fig. 4a and b) follow the same trend as that obtained for the phe-OMe in Fig. 3. In this way, as well as for phe-OMe, the tyr-OMe experimental  $^3J_{\text{HaHb}}$  and  $^3J_{\text{HaHc}}$  values vary with the solvent dielectric constant and

the theoretical calculations suggest that the conformer **Ia** and **Ib** population changes in these solvents are the main cause for this observed variation. Also, the energy (and population) and the C=O absorption values for tyr-OMe in acetonitrile and DMSO (Table 8) are almost the same as those obtained for phe-OMe (compare Tables 2 and 8 values), i.e., these two compounds have also the same behavior in solution.

The QTAIM molecular graphs shown in Fig. S6 (Supporting information), in the same way as phe-OMe, indicate that the tyr-OMe **V1a** and **V1c** conformers form intramolecular C–H...O interactions, which fulfill the Popelier criteria (Table 9). A C–H...O bond path for conformer **IIIc** was obtained, but this interaction is topologically very unstable (C–H...O bond ellipticity has a value of 16.735 au) and may be considered irrelevant. By applying the NBO analysis for tyr-OMe conformers (Table 10), one can obtain the same results as for phe-OMe: conformers with **c** geometry are, in general, the most unstable since they have the highest values of  $\Delta E_{\text{Lewis}}$  (related to steric effects), while conformers with **b** geometry are the most stable ones since they experience less steric effects than the other geometries ( $\Delta E_{\text{Lewis}}$  values, Table 10).

Therefore, phe-OMe and tyr-OMe show similar conformational behavior in both gas phase and in solution. The QTAIM and the NBO methods indicate that both steric effects and

**Table 8**Relative energies<sup>a</sup> (kcal mol<sup>-1</sup>), populations (percentage) for the tyr-OMe conformers in the gas phase (B3LYP/aug-cc-pVDZ) and by using the IEF-PCM implicit model in  $\text{CHCl}_3$ ,  $\text{CH}_3\text{CN}$  and DMSO. Theoretical (B3LYP/aug-cc-pVDZ) C=O stretching values are also showed.

Conformer	Isolated		THF		CH <sub>3</sub> CN		C=O <sup>1</sup>	DMSO		
	$\Delta E$	%P	$\Delta E$	%P	$\Delta E$	%P		$\Delta E$	%P	C=O <sup>2</sup>
<b>Ia</b>	0.00	20.8	0.00	27.2	0.00	20.8	1742.1	0.00	21.9	1732.4
<b>Ib</b>	0.19	15.2	0.30	16.2	0.07	18.3	1745.1	0.09	18.9	1735.9
<b>Ic</b>	0.18	15.4	0.76	7.5	0.66	6.8	1748.3	0.77	6.0	1739.1
<b>IIIb</b>	1.43	1.9	1.12	4.1	0.81	5.3	1731.2	0.85	5.2	1722.4
<b>IIIc</b>	0.89	4.6	1.44	2.4	1.56	1.5	1730.8	1.52	1.7	1720.5
<b>IV1a</b>	0.86	4.9	0.74	7.8	0.58	7.8	1750.8	0.55	8.7	1740.9
<b>IV1b</b>	0.08	18.1	0.34	15.4	0.16	16.0	1752.6	0.25	14.4	1744.0
<b>IV1c</b>	1.84	0.9	1.69	1.6	1.34	2.1	1754.6	1.31	2.4	1746.0
<b>IV2a</b>	2.84	0.2	3.01	0.2	1.42	1.9	1751.6	1.47	1.8	1742.5
<b>IV2b</b>	0.54	8.4	0.86	6.3	0.71	6.2	1748.4	0.75	6.1	1740.1
<b>V1a</b>	2.31	0.4	2.03	0.9	1.42	1.9	1751.0	1.41	2.0	1742.5
<b>V1b</b>	0.84	5.0	1.49	2.2	1.53	1.6	1747.6	1.55	1.6	1738.5
<b>V1c</b>	2.85	0.2	3.28	0.1	3.04	0.1	1730.7	3.02	0.1	1721.3
<b>V2a</b>	2.33	0.4	1.57	1.9	1.10	3.3	1748.9	1.17	3.0	1741.0
<b>V2b</b>	1.11	3.2	0.94	5.6	0.77	5.7	1740.6	0.82	5.5	1731.8
<b>V2c</b>	2.22	0.5	2.21	0.6	1.94	0.8	1734.9	2.05	0.7	1727.2

<sup>a</sup> ZPE corrections included.<sup>1</sup> It was applied correction factors (CF) with values of 0.998.<sup>2</sup> It was applied correction factors (CF) with values of 0.993.

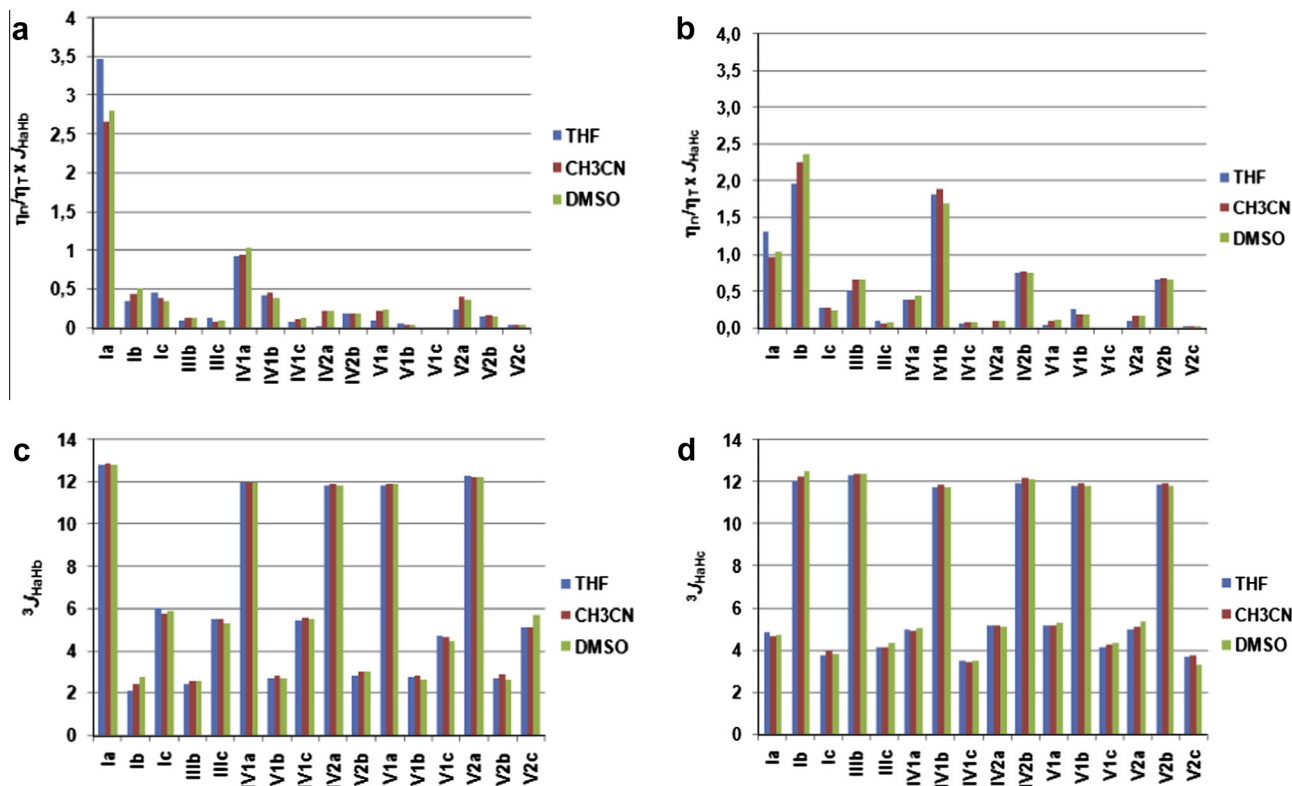


Fig. 4. Calculated (B3LYP/aug-cc-pVDZ level in the IEF-PCM implicit solvent model) tyr-OMe conformer parameter variations in different solvents for (a)  $\eta_T/\eta_T \times J_{\text{HaHb}}$ , (b)  $\eta_T/\eta_T \times J_{\text{HaHc}}$ , (c)  $^3J_{\text{HaHb}}$  and (d)  $^3J_{\text{HaHc}}$ .

Table 9

Popelier parameters applied to the tyr-OMe conformers which form CH...O interactions. The  $\rho_{\text{HBCP}}$ ,  $\nabla^2\rho_{\text{HBCP}}$  and all integration parameters obtained for hydrogen atoms are in atomic units (au). The conformer Ia is used as reference, since it cannot form a CH...O interaction.

Conformer	$\rho_{\text{HBCP}}$	$\nabla^2\rho_{\text{HBCP}}$	$q(\text{H})$	$E(\text{H})$	$M_1(\text{H})$	$V(\text{H})$
Ia	–	–	–0.006	–0.6161	0.131	50.791
V2a	0.007	+0.027	+0.031	–0.6045	0.122	46.193
V2c	0.006	+0.023	+0.017	–0.6092	0.124	47.499

Table 10

Full energy of the real system ( $\Delta E_{\text{FULL}}$ ), energy of the hypothetical case where hyperconjugation is removed ( $\Delta E_{\text{Lewis}}$ ) and hyperconjugative energy ( $\Delta E_{\text{hyper}}$ ) for the tyr-OMe conformers. Energy values in kcal mol<sup>–1</sup>.

	Ia	Ib	Ic	IIIb	IIIc	IV1a	IV1b	IV1c
$\Delta E_{\text{Full}}$	0.00	0.19	0.18	1.43	0.89	0.86	0.08	1.84
$\Delta E_{\text{Lewis}}$	5.88	2.99	8.42	4.03	10.98	7.33	9.92	11.05
$\Delta E_{\text{hyper}}$	7.59	4.36	9.96	4.13	11.88	8.03	11.45	10.70
	IV2a	IV2b	V1a	V1b	V1c	V2a	V2b	V2c
$\Delta E_{\text{Full}}$	2.84	0.54	2.31	0.84	2.85	2.33	1.11	2.22
$\Delta E_{\text{Lewis}}$	3.80	1.73	0.71	0.00	6.27	6.12	4.16	13.26
$\Delta E_{\text{hyper}}$	2.41	2.92	0.00	0.70	4.92	5.30	4.68	12.64

<sup>a</sup> ZPE corrections included.

hyperconjugative effects, and not IHB, are the main causes for the conformational preferences of these compounds.

## Conclusions

Amino ester derivatives instead of the amino acid themselves allow the study of these compounds in organic solvents by NMR, since they not exhibit the zwitterionic structure as an amino acid

does. In this way, by applying experimental <sup>1</sup>H NMR spectroscopy together with theoretical calculations, one may obtain a deeper understanding of the conformational behavior of these compounds in different solvents.

In particular, by comparing the theoretical and experimental phe-OMe and tyr-OMe  $^3J_{\text{HaHb}}$  and  $^3J_{\text{HaHc}}$  SSCCs value trends, it was possible to understand the conformational behavior of these compounds in solution. Indeed, by applying the QTAIM and NBO methods, it was highlighted that both steric and hyperconjugative effects, and not IHB, govern both the phe-OMe and tyr-OMe conformational preferences, mainly steric effects. Also, it was observed, both experimentally and theoretically, that the phe-OMe and tyr-OMe compounds are conformationally similar in both the gas phase and in solution. Thus, it was demonstrated that the hydroxyl group *para* positioned, which is the only structural difference between phe-OMe and tyr-OMe, has no significant conformational influence.

## Acknowledgements

The authors thank a Grant # 2012/03933-5, São Paulo Research Foundation (FAPESP) for providing financial support for this research, for a scholarship [to R.A.C. #2010/01170-1, FAPESP] and for a fellowship (to L.C.D. #2010/15764-4, FAPESP), and the authors thank CNPq for fellowships (to R.R. and CFT). Dr. T.R. Doi's assistance in revising this manuscript is also gratefully acknowledged.

## Appendix A. Supplementary material

Supplementary data associated with this article can be found, in the online version, at <http://dx.doi.org/10.1016/j.saa.2013.12.088>.

## References

- [1] J.T. Huang, D.J. Xing, W. Huang, *Amino Acids* 43 (2012) 567.
- [2] G.D. Chellapa, G.D. Rose, *Protein Sci.* 21 (2012) 1231.
- [3] B.C. Buer, B.J. Levin, E.N.G. Marsh, *J. Am. Chem. Soc.* 134 (2012) 13027.
- [4] Y. Hana, A. David, B. Liuc, J.G. Magadán, J.R. Bennink, J.W. Yewdell, S. Qian, *Proc. Natl. Acad. Sci. USA* 6 (2012) 1.
- [5] A. Lesarri, R. Sanchez, E.J. Cocinero, J.C. Lopez, J.L. Alonso, *J. Am. Chem. Soc.* 127 (2005) 12952.
- [6] B. Boeckx, G. Maes, *J. Phys. Chem. B.* 116 (2012) 12441.
- [7] C.H. Hu, M. Shen, H.F. Schaefer, *J. Am. Chem. Soc.* 115 (1993) 2923.
- [8] A.G. Császár, *J. Phys. Chem.* 100 (1996) 3541.
- [9] G. Von Helden, I. Compagnon, M.N. Blom, M. Frankowski, U. Erlekam, J. Oomens, B. Brauer, R.B. Gerber, G. Meijer, *Phys. Chem. Chem. Phys.* 10 (2008) 1248.
- [10] P. Echenique, J.L. Alonso, *J. Comput. Chem.* 29 (2008) 1408.
- [11] J.L. Alonso, E.J. Cocinero, A. Lessarri, M.E. Sanz, J.C. López, *Angew. Chem. Int. Ed.* 45 (2006) 3471.
- [12] W.D. Allen, H.F. Schaefer III, E. Czinki, A.G. Csa, V. Kasalova, *J. Comput. Chem.* 28 (2007) 1373.
- [13] A. Lesarri, E.J. Cocinero, J.C. Lopez, J.L. Alonso, *Angew. Chem. Int. Ed.* 43 (2004) 605.
- [14] H. Farrokhpour, F. Fathi, N.D. Brito, *J. Phys. Chem. A* 116 (2012) 7004.
- [15] M. Shmilovits-Ofir, Y. Miller, R.B. Gerber, *Phys. Chem. Chem. Phys.* 13 (2011) 8715.
- [16] G. Lee, *Bull. Korean Chem. Soc.* 33 (2012) 1561.
- [17] J.L. Alonso, I. Peña, J.C. López, V. Vaquero, *Angew. Chem.* 121 (2009) 6257.
- [18] H. Kayi, R.I. Kaiser, J.D. Head, *Phys. Chem. Chem. Phys.* 14 (2012) 4942.
- [19] R.A. Cormanich, L.C. Ducati, R. Rittner, *Chem. Phys.* 387 (2011) 85.
- [20] R.A. Cormanich, L.C. Ducati, R. Rittner, *J. Mol. Struct.* 1014 (2012) 12–16.
- [21] R.A. Cormanich, L.C. Ducati, C.F. Tormena, R. Rittner, *Chem. Phys.* 421 (2013) 32.
- [22] R.A. Cormanich, L.C. Ducati, C.F. Tormena, R. Rittner, *J. Phys. Org. Chem.* 421 (2013) 32.
- [23] C.J. Duarte, R.A. Cormanich, L.C. Ducati, R. Rittner, *J. Mol. Struct.* 1050 (2013) 174.
- [24] G. Albrecht, R.B. Corey, *J. Am. Chem. Soc.* 61 (1939) 1087.
- [25] J. Donohue, *J. Am. Chem. Soc.* 72 (1950) 949.
- [26] H.A. Levy, R.B. Corey, *J. Am. Chem. Soc.* 63 (1941) 2095.
- [27] S. Blanco, E.M. Sanz, J.C. López, J.L. Alonso, *Proc. Natl. Acad. Sci.* 104 (2007) 20183.
- [28] E.J. Cocinero, P. Villanueva, A. Lesarri, A.E. Sanz, S. Blanco, S. Mata, J.C. Lopez, J.L. Alonso, *Chem. Phys. Lett.* 435 (2007) 336.
- [29] E.J. Cocinero, A. Lesarri, J.U. Grabow, J.C. Lopez, J.L. Alonso, *Chem. Phys. Chem.* 8 (2007) 599.
- [30] R.F.W. Bader, *Atoms in Molecules: A Quantum Theory*, Clarendon, Oxford, 1990.
- [31] F. Weinhold, C.R. Landis, *Valency and Bonding*, Cambridge Univ. Press, Cambridge, 2005.
- [32] E. Cancès, B. Mennucci, J. Tomasi, *J. Chem. Phys.* 107 (1997) 3032.
- [33] V. Barone, in: D.P. Chong (Ed.), *Recent Advances in Density Functional Methods, Part I*, World Scientific Publ. Co., Singapore, 1996.
- [34] M.J. Frisch, G.W. Trucks, H.B. Schlegel, G.E. Scuseria, M.A. Robb, J.R. Cheeseman, J.A. Montgomery, Jr., T. Vreven, K.N. Kudin, J.C. Burant, J.M. Millam, S.S. Iyengar, J. Tomasi, V. Barone, B. Mennucci, M. Cossi, G. Scalmani, N. Rega, G.A. Petersson, H. Nakatsuji, M. Hada, M. Ehara, K. Toyota, R. Fukuda, J. Hasegawa, M. Ishida, T. Nakajima, Y. Honda, O. Kitao, H. Nakai, M. Klene, X. Li, J.E. Knox, H.P. Hratchian, J.B. Cross, V. Bakken, C. Adamo, J. Jaramillo, R. Gomperts, R.E. Stratmann, O. Yazyev, A.J. Austin, R. Cammi, C. Pomelli, J.W. Ochterski, P.Y. Ayala, K. Morokuma, G.A. Voth, P. Salvador, J.J. Dannenberg, V.G. Zakrzewski, S. Dapprich, A.D. Daniels, M.C. Strain, O. Farkas, D.K. Malick, A.D. Rabuck, K. Raghavachari, J.B. Foresman, J.V. Ortiz, Q. Cui, A.G. Baboul, S. Clifford, J. Cioslowski, B.B. Stefanov, G. Liu, A. Liashenko, P. Piskorz, I. Komaromi, R.L. Martin, D.J. Fox, T. Keith, M.A. Al-Laham, C.Y. Peng, A. Nanayakkara, M. Challacombe, P.M.W. Gill, B. Johnson, W. Chen, M.W. Wong, C. Gonzalez, J.A. Pople, *Gaussian 03, Revision E.01*, Gaussian Inc, Wallingford, CT, 2004.
- [35] A.K. Todd, AIMAll (Version 13.05.06), 2013 ([aim.tkgristmill.com](http://aim.tkgristmill.com)).
- [36] K. Ananda, V.V.S. Babu, *J. Peptide Res.* 57 (2001) 223.
- [37] Grams/AI v. 9.0, ThermoFisher, Woburn, MA, USA, 2009.
- [38] M. Karplus, *J. Chem. Phys.* 30 (1959) 11.
- [39] U. Koch, P.L.A. Popelier, *J. Phys. Chem.* 99 (1995) 9747.